VIP Solar Cells Very Important Paper

International Edition: DOI: 10.1002/anie.201503038
German Edition: DOI: 10.1002/ange.201503038

Pseudohalide-Induced Moisture Tolerance in Perovskite $CH_3NH_3Pb(SCN)_2I$ Thin Films**

*Qinglong Jiang, Dominic Rebollar, Jue Gong, Elettra L. Piacentino, Chong Zheng, and Tao Xu**

Abstract: *Two pseudohalide thiocyanate ions (SCN^-) have been used to replace two iodides in $CH_3NH_3PbI_3$, and the resulting perovskite material was used as the active material in solar cells. In accelerated stability tests, the $CH_3NH_3Pb(SCN)_2I$ perovskite films were shown to be superior to the conventional $CH_3NH_3PbI_3$ films as no significant degradation was observed after the film had been exposed to air with a relative humidity of 95% for over four hours, whereas $CH_3NH_3PbI_3$ films degraded in less than 1.5 hours. Solar cells based on $CH_3NH_3Pb(SCN)_2I$ thin films exhibited an efficiency of 8.3%, which is comparable to that of $CH_3NH_3PbI_3$ based cells fabricated in the same way.*

Perovskite-type $CH_3NH_3PbX_3$ solid-state solar cells with over 19% efficiency have recently been reported.[1] They represent promising candidates for next-generation photovoltaic devices owing to their astoundingly high efficiency, the low costs associated with their solution-based fabrication, and tunable optical properties.[2] Furthermore, this material performs very well in terms of both charge transport (electron/hole diffusion lengths of ca. 1 μm and 1.2 um, respectively, for $CH_3NH_3PbI_{3-x}Cl_x$),[3] and light absorption (1.5×10^4 cm^{-1} at 550 nm).[4] In general, perovskite solar cells are configured as a sandwich structure, and the photoanode morphologies affect the performance of the overall device.[5] Typically, a layer of three-dimensional (3D) TiO_2 is used as the photoanode with perovskite materials.[6] These 3D structures, acting as an electron-buffer, structure-supporting, and reflection layer, are filled up with a $CH_3NH_3PbX_3$ perovskite as the photovoltaically active layer, followed by capping with a layer of hole transport material (HTM) and a metal counter electrode, such as Au[6e] or Ag.[7]

Despite success in boosting their efficiency, perovskite solar cells are still facing several critical challenges, including stability issues,[8] the use of environmentally hazardous lead,[9] the expensive complex organic compounds in the HTM layer,[10] and the use of precious metals as the back cathode.[1,6e] Great efforts have been made to replace the lead with non-toxic tin,[9,11] the organic HTMs with cheaper inorganic HTMs,[10b] and the noble metal Au with cheaper metals, such as Ni.[12] In particular, perovskite materials decompose in moist air,[8b,13] which is the main barrier for their future commercialization. Only a handful of studies have been conducted to improve the stability of perovskite materials, for example by using $NH_2CH{=}NH_2PbI_3$ instead of $CH_3NH_3PbI_3$[14] and by changing the morphology of the perovskite material.[15] Herein, however, we describe a methods for the design of new perovskite materials that involves the replacement of the halide ions with pseudohalide ions.

Pseudohalides have similar chemical behaviors and properties to true halides.[16] In this study, we developed a new perovskite material, $CH_3NH_3Pb(SCN)_2I$, for perovskite solar cells by replacing two iodides in $CH_3NH_3PbI_3$ with two thiocyanate ions. As illustrated in Figure 1, two thirds of the I^- ions in traditional $CH_3NH_3PbI_3$ have been replaced by pseudohalide SCN^- ions.

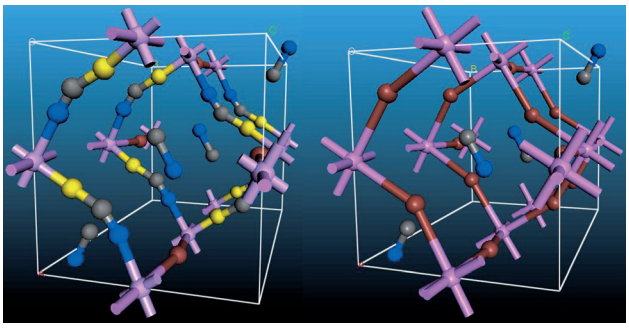

Figure 1. Perovskite structures of $CH_3NH_3Pb(SCN)_2I$ (left) and $CH_3NH_3PbI_3$ (right) for comparison. Carbon gray, iodine red, lead pink, nitrogen blue, sulfur yellow.

According to the crystal structure of $CH_3NH_3PbX_3$ perovskites, the lead and halide ions form the frame of the perovskite structure.[17] The first step of degradation in moisture involves the formation of a hydrated intermediate containing isolated PbX_6^{4-} octahedra.[13b] The formation constant of the lead halide complex is essentially its equilibrium constant, which reflects the binding tightness between the halides and the central Pb^{2+} ion. The formation constant K_4 (cumulative formation constant $\beta_n = K_1\times K_2\times \ldots K_n$) has been calculated to be only 3.5 for PbI_4^{2-},[18] which is in the range of the weak interactions between I^- and Pb^{2+}. In the case of $CH_3NH_3Pb(SCN)_2I$, the interaction between Pb^{2+} and SCN^- is much stronger, and the formation constant K_4 is up to 7 for $Pb(SCN)_4^{2-}$.[19] Comparing the spherical shape of I^- ions with the linear shape of SCN^- ions as indicated by their Lewis structures, the lone pairs of electrons from the S and N atoms in SCN^- can interact strongly with the Pb ion, which in turn

[*] Q. Jiang, D. Rebollar, J. Gong, E. L. Piacentino, Prof. C. Zheng, Prof. T. Xu
Department of Chemistry and Biochemistry
Northern Illinois University
DeKalb, IL 60115 (USA)
E-mail: txu@niu.edu

[**] Financial support from the U.S. NSF (CBET-1150617) is gratefully acknowledged.

Supporting information for this article is available on the WWW under http://dx.doi.org/10.1002/anie.201503038.

stabilizes the frame structure of $CH_3NH_3Pb(SCN)_2I$. We show that a direct improvement of moisture tolerance has been observed for $CH_3NH_3Pb(SCN)_2I$ in accelerated stability tests compared with the traditional $CH_3NH_3PbI_3$ perovskite material.

Figure 2 shows the X-ray diffraction (XRD) patterns of perovskite-type $CH_3NH_3Pb(SCN)_2I$ in comparison to with those of $CH_3NH_3PbI_3$, $Pb(SCN)_2$, and CH_3NH_3I (MAI). The XRD peaks (2θ) characteristic for the conventional perovskite $CH_3NH_3PbI_3$ are located at 14°, 20°, 29°, 32°, and 41°,[20] which are all present as expected. These peaks are also found for $CH_3NH_3Pb(SCN)_2I$, which strongly indicates that the

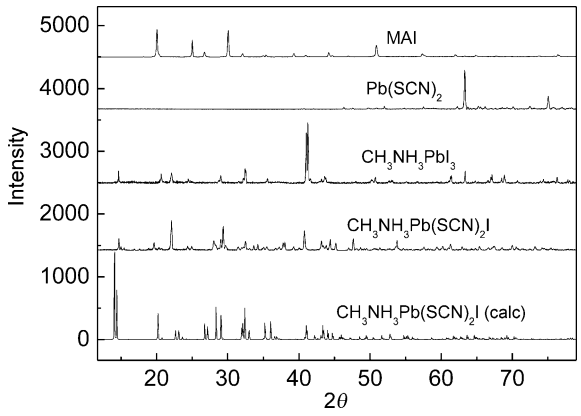

Figure 2. XRD patterns of the $CH_3NH_3PbI_3$ and $CH_3NH_3Pb(SCN)_2I$ perovskite materials.

$CH_3NH_3Pb(SCN)_2I$ material also has a perovskite structure. The calculated XRD pattern for $CH_3NH_3Pb(SCN)_2I$ matches well with the major experimentally determined XRD peaks. XRD patterns for $Pb(SCN)_2$ and MAI are also given in Figure 2 as references. The changes in the XRD patterns of both the $CH_3NH_3Pb(SCN)_2I$ and $CH_3NH_3PbI_3$ films resulting from exposure to air with 95% relative humidity are listed in the Supporting Information, Figure S2. No obvious changes could be observed for $CH_3NH_3Pb(SCN)_2I$ after four hours, whereas the XRD pattern of the $CH_3NH_3PbI_3$ film had severely deteriorated already after exposure to air with 95% relative humidity for 1.5 hours, as confirmed by the appearance of the peaks characteristic for PbI_2.

The accelerated moisture-tolerance tests for perovskite materials were performed by monitoring the reflection of the corresponding perovskite films in air with 95% relative humidity at room temperature. The increase in reflection for $CH_3NH_3PbI_3$ is due to the decomposition of the perovskite structure when subjected to moisture (Figure 3a).[8b] Perovskite-type $CH_3NH_3PbI_3$ started to decompose immediately after being exposed to moisture. After 1.5 hours, most of the black film had decomposed and turned yellow, which is due to the formation of PbI_2, and the corresponding reflection increased from approximately 10 to 20%. In the case of $CH_3NH_3Pb(SCN)_2I$ (Figure 3b), no obvious increase in reflection was observed even after exposure to moisture for four hours. The corresponding reflection increased by only 2% after four hours of exposure to moisture, from approximately 6 to 8%. Some very small white patches emerged at the corners, which are likely due to $Pb(SCN)_2$. Furthermore,

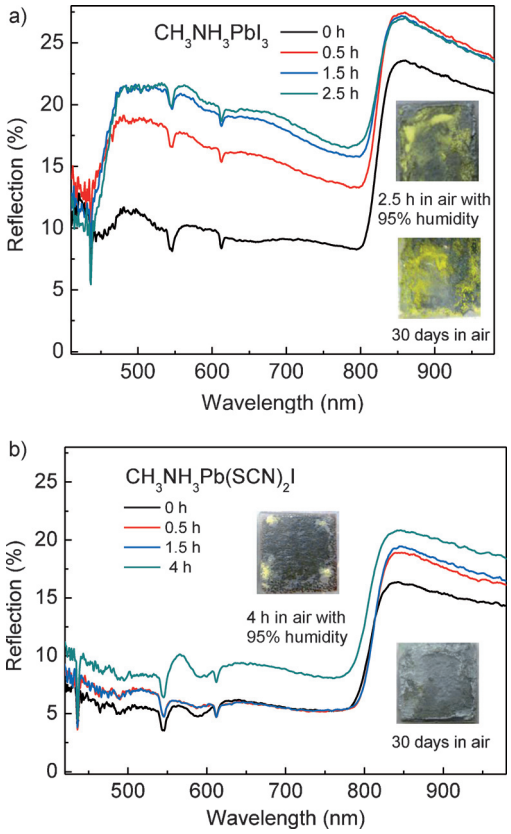

Figure 3. Accelerated stability tests with a) $CH_3NH_3PbI_3$ and b) $CH_3NH_3Pb(SCN)_2I$ in air with 95% relative humidity.

the black color of the $CH_3NH_3Pb(SCN)_2I$ film could last for months when the film was kept in air with a relative humidity of $\leq 40\%$. The bottom insets in Figure 3a and 3b show the $CH_3NH_3PbI_3$ and $CH_3NH_3Pb(SCN)_2I$ films, respectively, after 30 days in air with a relative humidity of 20–40%.

To gain further insights into the stability of the perovskite $CH_3NH_3Pb(SCN)_2I$ during the accelerated moisture-tolerance tests, the changes in the band gaps were also determined by plotting the square of the Kubelka–Munk function [$F(R_\infty) \times$ photon energy($h\nu$)] versus $h\nu$.[21] The band gap of $CH_3NH_3PbI_3$ was determined to be 1.504 eV, which is in accordance with previously reported values (Figure 4a).[20c,22] The band gap decreased to 1.470 eV after 2.5 hours, which indicates the decomposition of the $CH_3NH_3PbI_3$ perovskite structure in moisture, resulting in the formation of a mixture of $MAI{\cdot}H_2O$, $MAPbI_x$, $PbI_x{\cdot}H_2O$, and other iodide complexes.[8b,13] In contrast, $CH_3NH_3Pb(SCN)_2I$ exhibited a slightly wider band gap of 1.532 eV, which remained nearly the same after four hours of exposure to air with 95% relative humidity, suggesting that $CH_3NH_3Pb(SCN)_2I$ is a more stable perovskite structure (Figure 4b).

The presence of SCN groups in the material was further confirmed by total internal reflection Fourier transform infrared (TIR-FTIR) spectroscopy. Indeed, we observed the characteristic thiocyanate FTIR peak[23] at approximately 2050 cm^{-1} for both a pure $CH_3NH_3Pb(SCN)_2I$ film on glass and spin-coated $CH_3NH_3Pb(SCN)_2I$ on a TiO_2 nanoparticle photoanode (Figure S1). Furthermore, energy-dispersive X-ray spectroscopy (EDXS) measurements suggest that the

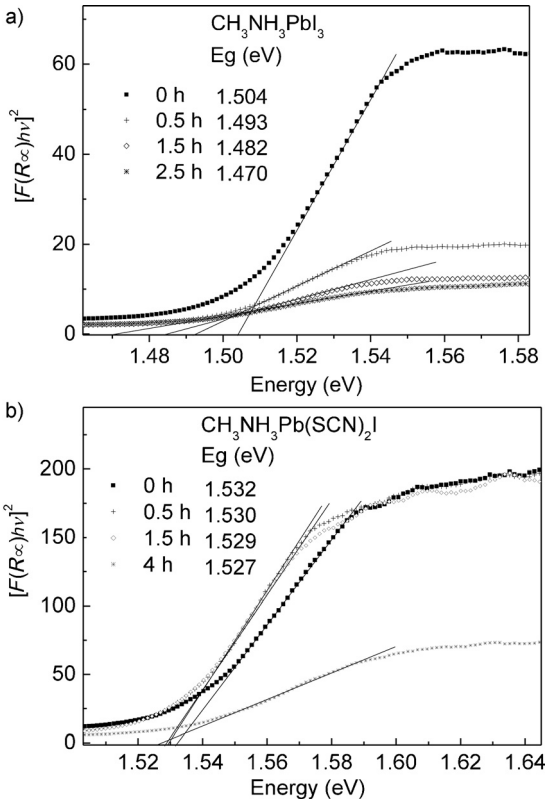

Figure 4. Tauc plots from accelerated stability tests with a) $CH_3NH_3PbI_3$ and b) $CH_3NH_3Pb(SCN)_2I$ in air with 95% relative humidity.

$CH_3NH_3Pb(SCN)_2I$ based device contains pronouncedly more sulfur than the $CH_3NH_3PbI_3$ based device. (Tables S1–S3). The sulfur in the $CH_3NH_3PbI_3$ based device originates from the HTM layer, which contains lithium bis(trifluoromethane)sulfonamide.

Scanning electron microscopy (SEM) images of the cross-sections of solar cells with $CH_3NH_3PbI_3$ and $CH_3NH_3Pb(SCN)_2I$ as the active materials are shown in Figure 5a and 5b, respectively. Both solar cells used an approximately 500 nm thick TiO_2 nanoparticle as the photoanode, a 200 nm thick HTM layer, and a 80 nm thick Au layer. No obvious morphological differences can be observed for these two solar cells.

The *J*–*V* curves of solar cells that are based on either $CH_3NH_3Pb(SCN)_2I$ or $CH_3NH_3PbI_3$ but use the same types of photoanodes, HTM layers, and Au counter electrodes and were prepared in our laboratory are compared in Figure 6. Apparently, $CH_3NH_3Pb(SCN)_2I$ exhibits a lower current density (15.1 mA cm^{-2}) than $CH_3NH_3PbI_3$ (21.1 mA cm^{-2}). However, the $CH_3NH_3Pb(SCN)_2I$ based cell displays better V_{oc} and FF values (V_{oc} = 0.87 V, FF = 0.63) than the $CH_3NH_3PbI_3$ based solar cell (V_{oc} = 0.80 V, FF = 0.52). The efficiencies of the two cells were relatively similar, namely 8.3% for the $CH_3NH_3Pb(SCN)_2I$ based cell and 8.8% for the $CH_3NH_3PbI_3$ based cell. Compared to the best reported efficiency for $CH_3NH_3PbI_3$ cells, the lower efficiency of our cells is mainly due to the low V_{oc} value, which is largely due to the crystallinity of the perovskite film, the quality of the interfaces, and the film engineering procedure. All of the

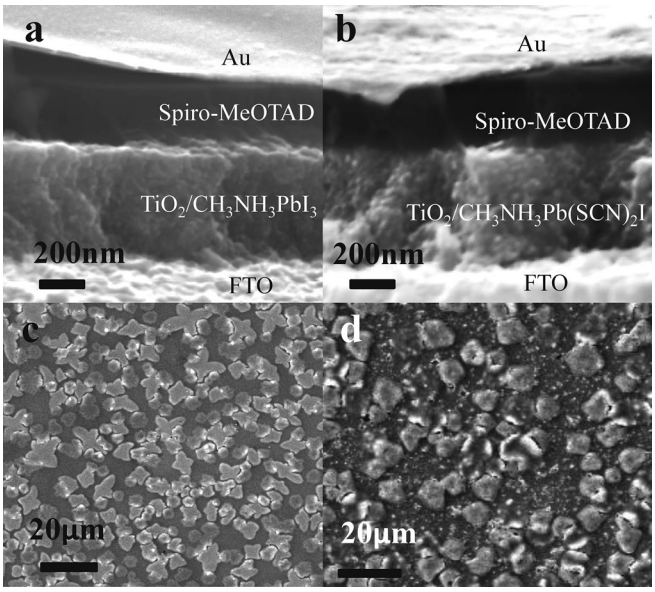

Figure 5. SEM images of perovskite solar cells. a, b) Cross-sections of $CH_3NH_3PbI_3$ (a) and $CH_3NH_3Pb(SCN)_2I$ (b) based solar cells. c, d) Top views of $CH_3NH_3PbI_3$ (c) and $CH_3NH_3Pb(SCN)_2I$ (d) based solar cells.

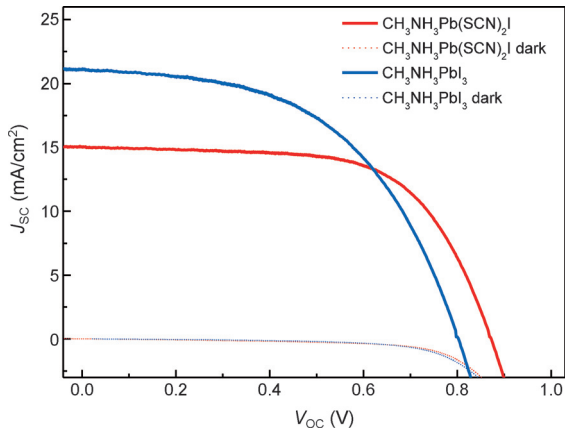

Figure 6. *J*–*V* curves of perovskite solar cells with $CH_3NH_3Pb(SCN)_2I$ or $CH_3NH_3PbI_3$ as the active layer.

critical parameters highlighting the photovoltaic performance of the devices are given in Table 1. The *J*–*V* curves of the cell made with $CH_3NH_3Pb(SCN)_2I$ that were recorded on the first day and on the 14th day after fabrication, and the corresponding curves of the cell made with $CH_3NH_3PbI_3$ on the first and seventh day are shown in Figure S3. The efficiency of the $CH_3NH_3PbI_3$ cell dropped from 8.8% on the first day to 6.9% on the seventh day; in contrast, the efficiency of the $CH_3NH_3Pb(SCN)_2I$ cell only dropped from 8.3% on the first day to 7.4% on the 14th day (Table S4), which thus exhibits a much better stability than the $CH_3NH_3PbI_3$ cell.

Table 1: Photovoltaic performance of solar cells with $CH_3NH_3Pb(SCN)_2I$ or $CH_3NH_3PbI_3$ as the active layer.

Cell	J_{sc} [mA cm^{-2}]	V_{oc} [V]	FF	η [%]	R_{sh} [Ω]	R_s [Ω]
$CH_3NH_3PbI_3$	21.1	0.80	0.52	8.8	555.0	19.1
CH_3NH_3 $Pb(SCN)_2I$	15.1	0.87	0.63	8.3	981.7	31.4

FF = fill factor, J_{sc} = short-circuit current density, V_{oc} = open-circuit voltage, R_s = series resistance, R_{sh} = shunt resistance.

In summary, we have developed a new type of perovskite material, $CH_3NH_3Pb(SCN)_2I$. The replacement of two iodides by two thiocyanate ions in a conventional $CH_3NH_3PbI_3$ material drastically improved the moisture tolerance of the resulting perovskite material.

Experimental Section

Synthesis of $Pb(SCN)_2$: An aqueous solution of $Pb(BF_4)$ (10 mL, Aldrich) and NaSCN (3.5 g, Aldrich) were mixed under stirring in deionized (DI) water (10 mL). The precipitate was filtered off and washed 6 times with DI water to obtain $Pb(SCN)_2$. CH_3NH_3I was synthesized as described previously.[6a] The $CH_3NH_3PbI_3$ precursor solution was prepared as follows: PbI_2 (0.289 g, Aldrich) and CH_3NH_3I (0.1 g) were dissolved in γ-butyrolactone (0.52 mL, Aldrich) at 60 °C under stirring for 3 h.[6a] The $CH_3NH_3Pb(SCN)_2I$ precursor solution was prepared as follows: $Pb(SCN)_2$ (0.203 g) and CH_3NH_3I (0.15 g) were dissolved in dimethylformamide (DMF, 0.6 mL) under stirring at 60 °C for 3 h. The HTM layer was prepared by dissolving 2,2′,7,7′-tetrakis(*N*,*N*-di-*para*-methoxyphenylamine)-9,9′-spiro-bifluorene (spiro-MeOTAD, 92 mg), lithium bis(trifluoromethane)sulfonamide (7.2 mg), and 4-*tert*-butylpyridine (12 mg), in chlorobenzene (1 mL).[6a]

The photoanodes were prepared as follows: Titanium(IV) bis(ethyl acetoacetato) diisopropoxide in 1-butanol (0.2 M) was sprayed on pre-cleaned FTO glass substrates at 400 °C, followed by sintering at 450 °C for 1 h to form a blocking layer. The electrodes were then soaked in $TiCl_4$ (0.2 M) in a sealed vial at 70 °C for 2 h,[6c] followed by sintering at 500 °C for 0.5 h. The resulting TiO_2/FTO electrodes were dipped into a solution of $H_2O_2/NH_3{\cdot}H_2O$ (9:1, v/v) for 20 s, and the substrates were then washed with DI water and ethanol. Finally, the electrodes were soaked in $TiCl_4$ (0.04 M) in a sealed vial at 70 °C for 1 h, and then heated to 500 °C for 0.5 h.

Fabrication of the corresponding perovskite solar cells: The perovskite precursor solution was spin-coated onto the photoanodes at 2000 rmp for 1 min in dry air, followed by annealing at 105 °C in air for 30 min. The HTM layer was spin-coated at 2500 rpm. An 80 nm thick Au film was thermally coated atop the HTM layer using an Edward 306 A thermal evaporator.

Characterization: A potentiostat (Gamry Reference 600) and a solar simulator (Photo Emission Inc. CA, model SS50B) were used to acquire the current density–voltage (*J*–*V*) curves. SEM images were taken on a Tescan scanning electron microscope (Vega II SBH). Diffusive reflectance measurements were conducted with a Filmetrics F20-EXR thin-film analyzer with an integrating sphere for measuring the reflectance. XRD spectra were collected on a Miniflex X-ray diffractometer. EDX spectra were recorded with a scanning electron microscope equipped with an INCAX-act Analytical Standard EDX Detector (Oxford Instruments). FTIR spectra were recorded with a reflective infrared spectrometer (ATI Mattson). Band-gap energies were calculated according to literature.[21] The calculation of the XRD patterns for $CH_3NH_3Pb(SCN)_2I$ was carried out using Accelrys MS modelling software (version 3.0.1).

Keywords: moisture tolerance · perovskite phases · pseudohalides · solar cells · thiocyanates

How to cite: *Angew. Chem. Int. Ed.* **2015**, *54*, 7617–7620
Angew. Chem. **2015**, *127*, 7727–7730

[1] Q. C. H. Zhou, G. Li, S. Luo, T.-b. Song, H.-S. Duan, Z. Hong, J. You, Y. Liu, Y. Yang, *Science* **2014**, *345*, 542–546.
[2] a) P. Gao, M. Grätzel, M. K. Nazeeruddin, *Energy Environ. Sci.* **2014**, *7*, 2448; b) H. J. Snaith, *J. Phys. Chem. Lett.* **2013**, *4*, 3623–3630; c) N. G. Park, *J. Phys. Chem. Lett.* **2013**, *4*, 2423–2429.
[3] S. D. Stranks, G. E. Eperon, G. Grancini, C. Menelaou, M. J. Alcocer, T. Leijtens, L. M. Herz, A. Petrozza, H. J. Snaith, *Science* **2013**, *342*, 341–344.
[4] S. Kazim, M. K. Nazeeruddin, M. Grätzel, S. Ahmad, *Angew. Chem. Int. Ed.* **2014**, *53*, 2812–2824; *Angew. Chem.* **2014**, *126*, 2854–2867.
[5] a) X. Feng, K. Zhu, A. J. Frank, C. A. Grimes, T. E. Mallouk, *Angew. Chem. Int. Ed.* **2012**, *51*, 2727–2730; *Angew. Chem.* **2012**, *124*, 2781–2784; b) Q. Jiang, F. Liu, T. Li, T. Xu, *J. Mater. Chem. C* **2014**, *2*, 618–621.
[6] a) Q. Jiang, X. Sheng, Y. Li, X. Feng, T. Xu, *Chem. Commun.* **2014**, *50*, 14720–14723; b) H. S. Kim, J. W. Lee, N. Yantara, P. P. Boix, S. A. Kulkarni, S. Mhaisalkar, M. Grätzel, N. G. Park, *Nano Lett.* **2013**, *13*, 2412–2417; c) A. Yella, L. P. Heiniger, P. Gao, M. K. Nazeeruddin, M. Grätzel, *Nano Lett.* **2014**, *14*, 2591–2596; d) M. M. Lee, J. Teuscher, T. Miyasaka, T. N. Murakami, H. J. Snaith, *Science* **2012**, *338*, 643–647; e) J. Burschka, N. Pellet, S. J. Moon, R. Humphry-Baker, P. Gao, M. K. Nazeeruddin, M. Grätzel, *Nature* **2013**, *499*, 316–320.
[7] M. Liu, M. B. Johnston, H. J. Snaith, *Nature* **2013**, *501*, 395–398.
[8] a) T. Leijtens, G. E. Eperon, S. Pathak, A. Abate, M. M. Lee, H. J. Snaith, *Nat. Commun.* **2013**, *4*, 2885; b) G. D. Niu, W. Z. Li, F. Q. Meng, L. D. Wang, H. P. Dong, Y. Qiu, *J. Mater. Chem. A* **2014**, *2*, 705–710.
[9] F. Hao, C. C. Stoumpos, D. H. Cao, R. P. H. Chang, M. G. Kanatzidis, *Nat. Photonics* **2014**, *8*, 489–494.
[10] a) P. Qin, S. Tanaka, S. Ito, N. Tetreault, K. Manabe, H. Nishino, M. K. Nazeeruddin, M. Grätzel, *Nat. Commun.* **2014**, *5*, 3834; b) J. A. Christians, R. C. Fung, P. V. Kamat, *J. Am. Chem. Soc.* **2014**, *136*, 758–764.
[11] M. H. Kumar, S. Dharani, W. L. Leong, P. P. Boix, R. R. Prabhakar, T. Baikie, C. Shi, H. Ding, R. Ramesh, M. Asta, M. Grätzel, S. G. Mhaisalkar, N. Mathews, *Adv. Mater.* **2014**, *26*, 7122–7127.
[12] Q. Jiang, X. Sheng, B. Shi, X. Feng, T. Xu, *J. Phys. Chem. C* **2014**, *118*, 25878–25883.
[13] a) A. Abate, M. Saliba, D. J. Hollman, S. D. Stranks, K. Wojciechowski, R. Avolio, G. Grancini, A. Petrozza, H. J. Snaith, *Nano Lett.* **2014**, *14*, 3247–3254; b) J. Yang, B. D. Siempelkamp, D. Liu, T. L. Kelly, *ACS Nano* **2015**, *9*, 1955–1963.
[14] a) N. J. Jeon, J. H. Noh, W. S. Yang, Y. C. Kim, S. Ryu, J. Seo, S. I. Seok, *Nature* **2015**, *517*, 476–480; b) J. W. Lee, D. J. Seol, A. N. Cho, N. G. Park, *Adv. Mater.* **2014**, *26*, 4991–4998.
[15] J. H. Kim, S. T. Williams, N. Cho, C.-C. Chueh, A. K. Y. Jen, *Adv. Energy Mater.* **2014**, 1401229.
[16] F. Bella, A. Sacco, G. P. Salvador, S. Bianco, E. Tresso, C. F. Pirri, R. Bongiovanni, *J. Phys. Chem. C* **2013**, *117*, 20421–20430.
[17] F. De Angelis, *Acc. Chem. Res.* **2014**, *47*, 3349–3360.
[18] H. L. Clever, F. J. Johnston, *J. Phys. Chem. Ref. Data* **1980**, *9*, 751–784.
[19] G. W. Leonard, M. E. Smith, D. N. Hume, *J. Phys. Chem.* **1956**, *60*, 1493–1495.
[20] a) Q. Chen, H. P. Zhou, T. B. Song, S. Luo, Z. R. Hong, H. S. Duan, L. T. Dou, Y. S. Liu, Y. Yang, *Nano Lett.* **2014**, *14*, 4158–4163; b) B.-w. Park, B. Philippe, T. Gustafsson, K. Sveinbjörnsson, A. Hagfeldt, E. M. J. Johansson, G. Boschloo, *Chem. Mater.* **2014**, *26*, 4466–4471; c) T. Baikie, Y. N. Fang, J. M. Kadro, M. Schreyer, F. X. Wei, S. G. Mhaisalkar, M. Grätzel, T. J. White, *J. Mater. Chem. A* **2013**, *1*, 5628–5641.
[21] X. T. Lu, Z. B. Zhuang, Q. Peng, Y. D. Li, *Chem. Commun.* **2011**, *47*, 3141–3143.
[22] J. H. Noh, S. H. Im, J. H. Heo, T. N. Mandal, S. I. Seok, *Nano Lett.* **2013**, *13*, 1764–1769.
[23] K. Ganesan, L. Ratke, *Soft Matter* **2014**, *10*, 3218–3224.

Received: April 1, 2015
Published online: May 12, 2015

